Europe PMC Funders Group
Author Manuscript
Nat Chem. Author manuscript; available in PMC 2022 May 18.

Published in final edited form as:
Nat Chem. 2021 December 01; 13(12): 1192–1199. doi:10.1038/s41557-021-00824-w.

Bottom-up fabrication of a proteasome-nanopore that unravels and processes single proteins

Shengli Zhang, **Gang Huang**, **Roderick Versloot**, **Bart Marlon Herwig Bruininks**, **Paulo Cesar Telles de Souza**, **Siewert-Jan Marrink**, **Giovanni Maglia***
Groningen Biomolecular Sciences & Biotechnology Institute, University of Groningen, 9747 AG Groningen, The Netherlands

Abstract

The precise assembly and engineering of molecular machines capable of handling biomolecules play crucial roles in most single-molecule methods. In this work, using components from all three domains of life, we fabricate an integrated multi-protein complex that controls the unfolding and threading of individual proteins across a nanopore. This 900 kDa multicomponent device was made in two steps. First, we designed a stable and low-noise β-barrel nanopore sensor by linking the transmembrane region of bacterial protective antigen to a mammalian proteasome activator. Then, an archaeal 20S proteasome was built into the artificial nanopore to control the unfolding and linearised transport of proteins across the nanopore. This multi-component molecular machine opens the door to two approaches in single-molecule protein analysis, in which selected substrate proteins are unfolded, fed to into the proteasomal chamber and then addressed either as fragmented peptides or intact polypeptides.

Introduction

Membrane-spanning channels and pores have key roles in cellular processes and in biotechnological applications such as nanopore DNA sequencing[1]. A nanopore protein sequencing device requires the unravelling of a protein and the recognition of individual amino acids by ionic currents as the polypeptide is transported across the nanopore. Several studies revealed that tiny differences between molecules can be identified by nanopore currents[2–7], suggesting that amino acid recognition should be a tractable problem. One of the main remaining challenges is to design a nanopore sensor capable of unfolding proteins without influencing the ionic signal[8,9]. Small transmembrane proteins have been designed to control the passive transport of ions across membranes, including a synthetic

Users may view, print, copy, and download text and data-mine the content in such documents, for the purposes of academic research, subject always to the full Conditions of use: https://www.springernature.com/gp/open-research/policies/accepted-manuscript-terms

*Corresponding author: g.maglia@rug.nl.

Author contribution
S.Z. and G.M. designed the experiments. G.M. supervised the project. S.Z. performed the experiments and data analysis. B.B., P.S., and S.M. conducted the simulation work. G.M. and S.Z. wrote the paper. All authors discussed the results, and commented on the manuscript.

Competing interest statement
Giovanni Maglia is a founder, a director and a shareholder of Portal Biotech Limited, a company engaged in the development of nanopore technologies. This work was not supported by Portal Biotech Limited.

Europe PMC Funders Author Manuscripts
Europe PMC Funders Author Manuscripts

Europe PMC Funders Author Manuscripts

Europe PMC Funders Author Manuscripts

ion channel[10], a four-helix divalent metal-ion transporter[11], membrane-spanning pores[12,13] and a DNA-scaffolded pore[14]. However, the ability to design nanopores with an integrated biopolymer handling unit has not been done. Such devices would add a new dimension to the protein engineering field, and allow designing next-generation nanopore sensors for biopolymer analysis. Advances in this field, nonetheless, have been hampered by a number of reasons. Usually, molecular machines form multimeric complexes that require complex post- and co-translational assembly[15]. The latter is particularly challenging because all components must be soluble, unprocessed by proteases, and co-expressed at similar levels. The introduction of artificial transmembrane regions provides an additional challenge as it reduces the solubility of the individual component and it can prevent proper assembly. Moreover, the design of the interface between the hydrophobic transmembrane polypeptides and the hydrophilic components remains unexplored. Finally, in order to obtain a functional device, the nanopore should remain constantly open and the operation of the molecular machine should not occlude the nanopore sensor.

In this work, we addressed all these challenges and fabricated in two steps a 42-component 900 kDa integrated nanopore sensor that consists of three co-assembled proteins. In the first step, aided by molecular dynamic simulations, we devise a strategy to design artificial nanopores from a soluble protein with a toroid shape (Fig. 1a-d). The designed synthetic nanopores showed an activity and electrical proprieties identical to the nanopores found in nature. In the second step, the multiprotein 20S proteasome from *Thermoplasma acidophilum* [16] was incorporated into the artificial nanopore (Fig. 1e-h). This design allows two approaches to single-molecule protein analysis including sequencing. In the chop-and-drop mode, unfolded proteins are first degraded by the proteasome and the resulting fragment delivered to the nanopore. In the thread-and-read mode, intact substrates are detected as they translocate across the nanopore. Notably, the activity of the proteasome and the unfolding of proteins did not have an influence on the ionic signal.

Results and Discussion

Design of transmembrane proteins

In cells, heptameric proteasome activator 28α regulates the function of the proteasome by docking on the heptameric 20S core proteasome particle[17]. Hence, in the first step to build a proteasome-nanopore, we designed a nanopore based on the proteasome activator 28α (also called REG or 11S activators[18], *Mus musculus*, Fig. 1a and Fig. 2a). The disorder region of REG (from P64 to P100) was replaced with the β-barrel transmembrane region (VHGNAEVHASFFDIGGSVSAGF) of the heptameric anthrax protective antigen nanopore[19] (PA, *Bacillus anthracis*, Fig. 2a and Supplementary Fig. 1). A β-barrel transmembrane region was chosen because it offers high thermodynamic stability and can tolerate many sequences substitutions[20,21]. A short flexible and hydrophilic linker (SSG) was added to each side of the β-barrel (Fig. 1a-d, Fig. 2a, and Supplementary Fig. 1) in order to mediate the interaction between the transmembrane part of anthrax protective antigen and REG, and to provide a passage for the ion to enter the nanopore.

Despite the 22 residues of this transmembrane (TM) region are sufficient to span the hydrophobic core of a lipid bilayer, the initial construct did not insert into lipid bilayer

Europe PMC Funders Author Manuscripts

Europe PMC Funders Author Manuscripts

(Fig. 2b). Since the length of the linker is likely to play an essential role in guiding membrane insertion and in controlling the transmembrane ionic transport, we tested one deletion mutant (Δ2) and five insertion mutants (∇2, ∇4, ∇8, ∇12, and ∇16, Fig. 2b). With the exception of Δ2, all variants could insert into the lipid bilayer, although with different efficiency. ∇8, ∇12, and ∇16 showed large current fluctuations, which prevented nanopore characterization (Supplementary Fig. 2). ∇4 showed full current blocks and a heterogeneous unitary conductance (Fig. 2c). Among all constructs tested, ∇2, which was efficiently expressed and purified (Supplementary Fig. 3), produced uniform pores in lipid bilayers with mean unitary conductance (1.17 ± 0.14 nS at -35 mV, 1 M NaCl, 15 mM Tris, pH 7.5, n = 59, Fig. 2d). Remarkably, ∇2-REG-PA-nanopore (hereafter REG-nanopore) inserted as efficiently and as uniformly as other nanopores found in nature (*e.g.* alpha hemolysin[22]), and remained open indefinitely into the lipid bilayer (Supplementary Fig. 4a). The individual peptides corresponding to the TM region of anthrax protective antigen could not form nanopores, indicating that a soluble scaffold is required to stabilize the nanopore in lipid bilayers. TEM images showed that the REG-nanopores assemble into oligomers (Supplementary Fig. 5a).

In order to validate this design principle, we first generalised the linker sequence. We found that amino acid substitutions with serine residues were well tolerated (Fig. 2e). Hence, the β-barrel sequence elongated by linkers containing five serine residues was introduced in two additional soluble proteins. The first was a AAA+ ATPase domain of *Aquifex aeolicus*, which activates the transcription σ54-RNA polymerase[23] (Fig. 2f and Supplementary Fig. 1). The second was PA26, a proteasome activator from *Trypanosoma brucei* [18] (Fig. 2g and Supplementary Fig. 1). Despite both proteins had a different diameters and surface residues, they inserted into lipid bilayers forming open nanopores, indicating that the β-barrel transmembrane domain and a five-amino acid hydrophilic linker allows a generic method to introduce soluble proteins into lipid bilayers for biopolymer analysis. REG was preferred to PA26 as the latter occasionally closed in planar lipid bilayers (Fig. 2g).

Functional properties of the optimized artificial nanopore

Molecular dynamics (MD) simulations were performed on the REG-nanopores construct to better understand the electrostatic and hydrophobic Interactions between the nanopore and the lipid bilayer. As shown in Fig. 2a and Fig. 3a, two rings of hydrophobic residues anchor the TM region to the hydrophobic edges of the bilayer, while alternated residues with aliphatic side-chains interface the core of the bilayer. The lumen of the pore is kept hydrated by hydrophilic residues. As expected, the hydrophilic side-chain of the linker residues are interacting with the charged head groups of membrane lipids. Inside the β-barrel region, the REG-nanopore showed an increased occupancy of cations compared to anions (Supplementary Fig. 6). Similar to other β-barrel nanopores such as αHL[22], REG-nanopores showed an asymmetric current–voltage (*I–V*) relationship (Fig. 3b,c). Ion-selectivity measurements using asymmetric NaCl concentrations (0.5 M/*trans* and 2.0 M/*cis*) confirmed the nanopore is cation selective (P_{Na^+}/P_{Cl^-} = 1.90 ± 0.18, Fig. 3d). Here and throughout the manuscript, uncertainties indicate the standard deviations obtained from at least three experiments. The correct folding of the REG-nanopore in the lipid bilayer was characterized using cyclodextrins (CDs), circular molecules that

Europe PMC Funders Author Manuscripts

Europe PMC Funders Author Manuscripts

binds to β-barrel nanopores[24]. α-CD, β-CD and γ-CD were added to the *cis* side of the artificial nanopore and the magnitude of the ionic current associated with a blockade (I_B) was measured. It was reported that only β-CD and γ-CD can block anthrax protective antigen nanopores[25], presumably because α-CD translocates too quickly to be observed. Accordingly, α-CD blockades were not observed (Supplementary Fig. 7a). β-CD induced fast blockades (spikes), most likely reflecting a fast transport across the nanopore (Fig. 3e). γ-CD showed characteristic blockades (Fig. 3f). Recordings with the αHL nanopore showed that imipramine induce additional blockades when added to the solution[24], reflecting the binding of the analyte to CD molecules inside the nanopore. Accordingly, REG-nanopores also showed additional analyte blockades in the presence of γ-CD (Fig. 3g), and reduced average spike current values of the blockades induced by β-CD (Supplementary Fig. 7b-d), indicating a binding between the CD adaptors and the analyte. Finally, the ability of the nanopore to identify peptides was tested using angiotensin I (10 amino acids, net charge 0) and dynorphin A (17 amino acids, net charge +4). We found that the two peptides induced blockades which could be distinguished in mixture using several parameters, including the residual current and the duration of the current blockades (Fig. 3h-j). Peptides smaller than angiotensin II (8 amino acids, net charge 0) could not be observed by nanopore recordings (Supplementary Fig. 7e), thus providing an approximative detection limit of oligopeptide detection using REG-nanopore.

Building a proteasome-nanopore

In the second and final step, the REG-nanopore is fused with the 20S proteasome from *Thermoplasma acidophilum.* The latter is made by four stacked rings composed of 14 α- and 14 β-subunits (Fig. 1e and Fig. 1f)[16]. The two-flanking outer α-rings allow for the association of the 20S proteasome with several regulatory complexes[26], among which is proteasome activator REG (Fig. 1a)[27]. We found, however, that when the proteasome was added to the *cis* side of individual REG-nanopore, no clear interaction was observed. This is most likely because the high ionic strength used (1 M NaCl) does not allow such interaction[28]. The crystal structure of the *Thermoplasma acidophilum* proteasome in complex with PA26 from *Trypanosoma* brucei[18], a homolog of REG, shows that the carboxy-terminal tails of PA26 slide into a pocket on the 20S proteasome, near the amino-terminus of the α-subunit (Fig. 4a). Hence, we fused the C-terminal of REG (Y249 in REG corresponding to S231 in PA26, Fig. 4a) with L21 of a proteasome α-subunit, in which the first 20 residues are removed (Δ20-α-subunit), leaving the proteasome gate open towards the REG-nanopore. The formation of the proteasome requires co-assembly of the α and β-subunits. Thus, REG-nanopore fused to proteasome Δ20-α-subunit (REGαΔ20 nanopore) containing a C-terminal His-tag, a second opened proteasomal subunit (αΔ12, where the first 12 residues are removed allowing the fast degradation of unfolded substrates without the need for a proteasome activator[29]) containing a C-terminal Strep-tag, and the proteasome β-subunit were co-expressed in *E. coli* cells using a two-vector system (**Extended Methods in Supporting Information** and Fig. 4b). Although all proteins could be expressed, SDS analysis indicated that the proteasome-nanopore was proteolytically cleaved inside *E. coli* cells during expression (Supplementary Fig. 8b). Proteolysis was prevented by optimizing the linker length between the REG-nanopore and α-subunit and by introducing a poly-histidine at the N-terminus of the REG-nanopore. The latter was

Europe PMC Funders Author Manuscripts

Europe PMC Funders Author Manuscripts

introduced to shield the linker between subunits from cellular proteases (Supplementary Fig. 8d). A co-assembled proteasome-nanopore (mutant 8, Supplementary Fig. 8 and 9) was then purified in two steps by affinity chromatography (Extended Methods in Supporting Information and Fig. 4b). SDS-PAGE, native PAGE, TEM, and LC-MS/MS confirmed the successful assembly of the multi-protein complex (Fig. 4d, Fig. 4e, Supplementary Fig. 5 and Supplementary Fig. 10-12). Activity assays revealed that the proteasome-nanopore was active, with the proteolytic activity increasing with the temperature, and decreasing with the salt concentration (Supplementary Fig. 13). The transmembrane proteasome inserted efficiently in lipid bilayers, while the spontaneous release from the lipid bilayer was not observed (Supplementary Fig. 4b). The proteasome-nanopores showed low-noise current recordings at negative applied potentials (Fig. 4c). However, at applied potentials higher than +20 mV the proteasome-nanopore often gated (Supplementary Fig. 14). The different electrical properties allowed distinguishing REG-nanopores from proteasome-nanopores, and allowed establishing that the subunits of the proteasome-nanopores did not disassembled during the electrical recordings (Supplementary Fig. 15). The *I-V* curve of the proteasome-nanopore was similar to that of REG-nanopore and to that of a proteasome-nanopore with a closed gate[29] (the latter maintains the N-terminals region of the α subunits atop of the REG-nanopore, which keeps the entry of the nanopore closed, Supplementary Fig. 16a). Similarly, the ion selectivity (Supplementary Fig. 16b) and the electrical noise of the proteasome-nanopore were also similar to that of REG-nanopore (Supplementary Fig. 16c-e). These lines of evidence indicate that the transmembrane region of the proteasome-nanopore was unchanged compared to the REG-nanopore, and that the proteasome above the nanopore does not influence the ionic signal (see additional discussion in supporting information).

Real-time protein processing

The activity of the transmembrane proteasome was tested using substrates containing a C-terminal ssrA tag, which mediates the interaction with VAT (Valosin-containing protein-like ATPase of *Thermoplasma acidophilum*)[30]. The latter is a processive hand-over-hand unfoldase that pulls on two extended residues of substrates through the proteasome chamber[31]. Here, we used VATΔN[32], in which the first 183 amino acids of the N-terminal domain corresponding to a regulatory domain were deleted (Supplementary Fig. 17). VATΔN displays higher unfolding activity than wild type VAT. We tested two substrates. The first, named S1 (123 amino acid residues), was designed to be unstructured. It contained an ssrA tag followed by four stretches of 15 serine residues, each flanked by 10 arginine residues and three hydrophobic residues (FYW, Supplementary Fig. 18). The polyarginine residues were introduced to induce the electrophoretic transport across the nanopore, while the hydrophobic residues are ideal targets for the proteolytic activity of the proteasome[33]. The ssrA tag was introduced to allow VATΔN recognition[32]. 'Superfolder' green fluorescent protein (GFP)[34], which modified by adding 10 arginines and a ssrA tag at the C-terminus (Supplementary Fig. 18), was also tested. GFP was selected because of it high stability towards temperature denaturation (melting temperature 78 °C[35]) and chemotropic agents (unfolding at more than 4M Gu.HCl[36]), hence providing a good model system to test the limit of the proteasome-nanopore to unfold proteins. The activity of VATΔN was optimized using bulk assays (Supplementary Fig. 19). Hereafter, experiments were performed at 40 °C

Europe PMC Funders Author Manuscripts

Europe PMC Funders Author Manuscripts

in 1 M NaCl, 15 mM Tris-HCl, pH 7.5, 20 mM $MgCl_2$ solutions. Tests were performed using either proteolytic active or inactive proteasome-nanopores. In the latter, the amino-terminal threonine 1 in the active site was replaced with alanine[15,37].

Thread-and-read

Two approaches to study single proteins become possible by using the proteasome-nanopore fabricated in this work. In the first, named thread-and-read, proteins are unfolded by VATΔN and thread across inactivated proteasome. The linearized polypeptide then translocates across the nanopore by the action of the electroosmotic flow. We tested this approach using S1 and GFP at 40 °C and -30 mV in 1 M NaCl, 15 mM Tris, pH 7.5. The addition of folded GFP to the cis side of a proteasome-nanopore induced no blockades. By contrast, the addition of unfolded and poly-charged S1 induced many blockades that showed a residual current (I_{res}, defined as the percent ratio between the blocked nanopore current the open nanopore current) of 7.3 ± 0.1% (Supplementary Fig. 20b and Supplementary Fig. 21b). The blockades were either short (dwell time: 0.30 ± 0.01 ms) or second-long (Supplementary Fig. 20b, Supplementary Fig. 21b and Supplementary Table 1). Most likely, the shorter blockades reflect the translocation of S1 across the proteasome-nanopore and the long blockades reflect the occlusion of the proteasome chamber by the substrate. The reduced dwell time of S1 with increasing voltage (Supplementary Fig. 21) indicates that S1 translocate across the nanopore[38]. When an equal concentration of VATΔN and substrate protein in the presence of 2.0 mM ATP were added to the solution, S1 blockades became longer (6.64 ± 0.21 ms) and the I_{res}% increased about ten-fold (70.2 ± 1.0, Fig. 5a, Supplementary Fig. 20 and Supplementary Fig. 22), most likely reflecting the VATΔN-assisted and stretched translocation of S1 across the nanopore. In the presence of VATΔN and ATP, GFP blockades were also observed (Fig. 5b, Supplementary Fig. 23, and Supplementary Fig. 24), indicating that the unfoldase linearized and fed the substrate protein through the nanopore. GFP blockades were not observed in the absence of either VATΔN or ATP, or when PAN[39] unfoldase or WT-VAT (WT-VAT contains an N-terminal domain that inhibits its unfolding activity[32]) were used instead of VATΔN (Supplementary Fig. 25). When the ATP concentration was increased to 6.0 mM the average dwell time of GFP blockades decreased to 2.4 ± 1.7 ms (Supplementary Fig. 26), suggesting that VATΔN is capable of feeding the polypeptide through the nanopore at a speed that can be tuned by the concentration of ATP. Contrary to S1 blockades, VATΔN-assisted GFP blockades showed I_{res}% close to zero, suggesting the formation of secondary structures of the substrate protein inside the proteasomal chamber after VATΔN-unfolding and before translocating across the nanopore. In the presence of 1 M urea, GFP current blockades became similar to the blockades induced by unstructured S1 (dwell time: 7.8 ± 1.7 ms, I_{res}%: 70.3 ± 0.9, Fig. 5a, Fig. 5c, Supplementary Fig. 22 and Supplementary Fig. 27). Most likely, urea prevented the partial refolding of the substrate allowing a stretched translocation across the nanopore after GFP was unfolded by VATΔN at the top of proteasome-nanopore. Although a stretched translocationacross the nanopore is an important achievemnt, the electrical signal of individual events was relatively heterogeneous (Fig. 5a-c and Supplementary Fig. 22, 24, 26 and 27) and the identification of amino acids was not attainable. The latter might become possible by using a nanopore with sub-nanometer diameter, such as heptameric FraC[3], possibly coupled with a more uniform electroosmotic transport across the nanopore.

Europe PMC Funders Author Manuscripts

Europe PMC Funders Author Manuscripts

Nonetheless, an important finding was that the unfolding of the protein above the nanopore did not affect the ionic signal (supporting information for a more detailed discussion), indicating that the ionic signal can be entirely used for polypeptide identification.

Chop-and-drop

The enclosed architecture of the VATΔN-proteasome-nanopore allows a fundamentally new approach in single-molecule nanopore protein analysis, in which the proteasome cleaves an unfolded protein and the resulting peptides are recognized as they translocate the nanopore. We recently showed that the ionic signal from peptide blockades to a FraC nanopore relate directly to the volume of the peptide[3,4]. Hence, a proteasome-nanopore might be used as the equivalent of protein fingerprinting by mass spectrometry, but at the single-molecule level. We tested this approach using S1 and GFP. When an active proteasome-nanopore was used, the second-long blockades observed during unassisted S1 translocation disappeared, while the short blockades became faster (0.20 ± 0.01 ms, Fig. 5d and Supplementary Fig. 28a). These results suggest, therefore, that the proteasome processes the substrates as they translocate across the nanopore. When VATΔN and ATP were added in solution, more spaced and shorter blockades were observed (Fig. 5e and Supplementary Fig. 28b), indicating that the reduced speed of polypeptide threading across the proteasomal chamber allowed the degradation of S1 into smaller peptides that are quickly transported across the nanopore. Accordingly, when GFP was tested under the same conditions yet fewer blockades were observed. The size-limit of peptide detection of the REG-nanopore is ~10 amino acids (Fig. 3h-j and Supplementary Fig. 7e), while the proteasome has been shown to produce peptide fragments between ~6 and ~10 amino acids depending on the protein substrate[40]. In turn this suggests that the slower unfolding of GFP compared to the unstructured S1 allowed for a more efficient proteolysis of the substrate into yet smaller peptides (Fig. 5e-f), which are transported across the nanopore too quickly to be observed. Although further improvements will be required for allowing single-molecule fingerprinting (*e.g.* changing the nanopore size or tuning the proteolytic pattern of the proteasome), this work present the first important demonstration that small molecule products of an enzymatic reaction can be addressed by a nanopore.

In conclusion, this work describes a strategy to build nanopores with advanced functionalities. Soluble proteins with a toroidal shape can be inserted into a lipid membrane by replacing a loop on the protein surface with the transmembrane region of a β-barrel pore flanked by a short hydrophilic linker. The artificial nanopores inserted efficiently into lipid bilayers and showed a well-define β-barrel structure. Bespoke optimizations of the length and composition of the hydrophilic linker allowed to engineer a nanopore that displayed low current noise and remained constantly open under an applied potential. Using this approach, we fabricated from the bottom up a 42-protein component nanopore sensor that is capable of processing folded proteins. This multi-protein molecular machine opens the door to two new potential approaches in single-molecule protein characterization, in which individual proteins are addressed by a nanopore either as intact linearized polypeptides or as a pattern of fragmented peptides.

Europe PMC Funders Author Manuscripts

Europe PMC Funders Author Manuscripts

Methods

A detailed description of the methodology can be found in the Supplementary Information. A short description is given here.

General materials

Oligonucleotides and gBlock gene fragments were obtained from Integrated DNA Technologies (IDT). All enzymes were purchased from Fisher Scientific. All peptides and chemicals were obtained from Sigma-Aldrich. 1,2-diphytanoyl-sn-glycero-3-phosphocholine (DPhPC) was purchased from Avanti Polar Lipids.

Plasmid Construction for proteins

All gBlock gene fragments were ordered for synthesis by IDT. Plasmid and gene were ligated together using T4 ligase (Fermentas). The identity of the clones was confirmed by sequencing at Macrogen.

Data recordings and analysis

Current recordings were performed in a planar bilayer set-up as described previously[41]. Electronic signals were recorded by using an Axopatch 200B (Axon Instruments) with digitization performed with a Digidata 1440 (Axon Instruments). Clampex 10.7 software and Clampfit 10.7 software (Molecular Devices) were used for electronic signal recording and subsequent data analysis, respectively. Events were collected using the single-channel search feature in Clampfit.

Supplementary Material

Refer to Web version on PubMed Central for supplementary material.

Aknowlegements

This work is financially supported by ERC consolidator grant (number: 726151).

Data availability

All relevant data are included in the article and its Supplementary Information. Statistical source data, unmodified gels, and molecular dynamics simulations results are provided in Source data. Data is also available from the authors upon reasonable request.

References

1. Bayley H. Nanopore Sequencing: From Imagination to Reality. Clin Chem. 2014; 61 :25. [PubMed: 25477535]
2. Kang XF, Cheley S, Guan X, Bayley H. Stochastic detection of enantiomers. J Am Chem Soc. 2006; 128 :10684–10685. [PubMed: 16910655]
3. Huang G, Voet A, Maglia G. FraC nanopores with adjustable diameter identify the mass of opposite-charge peptides with 44 dalton resolution. Nat Commun. 2019; 10 :1–10. [PubMed: 30602773]

Europe PMC Funders Author Manuscripts

4. Huang G, Willems K, Soskine M, Wloka C, Maglia G. Electro-osmotic capture and ionic discrimination of peptide and protein biomarkers with FraC nanopores. Nat Commun. 2017; doi: 10.1038/s41467-017-01006-4
5. Restrepo-Pérez L, Wong CH, Maglia G, Dekker C, Joo C. Label-Free Detection of Post-translational Modifications with a Nanopore. Nano Lett. 2019; doi: 10.1021/acs.nanolett.9b03134
6. Ouldali H, et al. Electrical recognition of the twenty proteinogenic amino acids using an aerolysin nanopore. Nature Biotechnology. 2020; doi: 10.1038/s41587-019-0345-2
7. Hu Z-L, Huo M-Z, Ying Y-L, Long Y-T. Biological Nanopore Approach for Single-Molecule Protein Sequencing. Angew Chemie. 2020; doi: 10.1002/ange.202013462
8. Nivala J, Mulroney L, Li G, Schreiber J, Akeson M. Discrimination among protein variants using an unfoldase-coupled nanopore. ACS Nano. 2014; doi: 10.1021/nn5049987
9. Nivala J, Marks DB, Akeson M. Unfoldase-mediated protein translocation through an α-hemolysin nanopore. Nat Biotechnol. 2013; doi: 10.1038/nbt.2503
10. Xu C, et al. Computational design of transmembrane pores. Nature. 2020; doi: 10.1038/s41586-020-2646-5
11. Joh NH, et al. De novo design of a transmembrane zn2+-transporting four-helix bundle. Science (80-). 2014; doi: 10.1126/science.1261172
12. Lu P, et al. Accurate computational design of multipass transmembrane proteins. Science (80-). 2018; doi: 10.1126/science.aaq1739
13. Scott A, Niitsu A, Kratochvil H, Chemistry EL-N. Constructing ion channels from water-soluble α-helical barrels. nature com. 2021
14. Spruijt E, Tusk SE, Bayley H. DNA scaffolds support stable and uniform peptide nanopores. Nat Nanotechnol. 2018; 13 :739–745. [PubMed: 29808001]
15. Seemüller E, et al. Proteasome from Thermoplasma acidophilum: a threonine protease. Science. 1995; 268 :579–82. [PubMed: 7725107]
16. Löwe J, et al. Crystal structure of the 20S proteasome from the archaeon T. acidophilum at 3.4 Å resolution. Science (80-). 1995; 268 :533–539.
17. Sugiyama M, et al. Spatial arrangement and functional role of α subunits of proteasome activator PA28 in hetero-oligomeric form. Biochem Biophys Res Commun. 2013; doi: 10.1016/j.bbrc.2013.01.071
18. Förster A, Masters EI, Whitby FG, Robinson H, Hill CP. The 1.9 Å structure of a proteasome-11S activator complex and implications for proteasome-PAN/PA700 interactions. Mol Cell. 2005; 18 :589–599. [PubMed: 15916965]
19. Jiang J, Pentelute BL, Collier RJ, Hong Zhou Z. Atomic structure of anthrax protective antigen pore elucidates toxin translocation. Nature. 2015; 521 :545–549. [PubMed: 25778700]
20. Cheley S, Braha O, Lu X, Conlan S, Bayley H. A functional protein pore with a “retro” transmembrane domain. Protein Sci. 1999; doi: 10.1110/ps.8.6.1257
21. Gu LQ, et al. Reversal of charge selectivity in transmembrane protein pores by using noncovalent molecular adapters. Proc Natl Acad Sci U S A. 2000; 97 :3959–3964. [PubMed: 10760267]
22. Maglia G, Restrepo MR, Mikhailova E, Bayley H. Enhanced translocation of single DNA molecules through α-hemolysin nanopores by manipulation of internal charge. Proc Natl Acad Sci U S A. 2008; doi: 10.1073/pnas.0808296105
23. Chen B, et al. Engagement of Arginine Finger to ATP Triggers Large Conformational Changes in NtrC1 AAA+ ATPase for Remodeling Bacterial RNA Polymerase. Structure. 2010; doi: 10.1016/j.str.2010.08.018
24. Gu LQ, Braha O, Conlan S, Cheley S, Bayley H. Stochastic sensing of organic analytes by a pore-forming protein containing a molecular adapter. Nature. 1999; 398 :686–690. [PubMed: 10227291]
25. Yannakopoulou K, et al. Symmetry requirements for effective blocking of pore-forming toxins: Comparative study with α-, β-, and γ-cyclodextrin derivatives. Antimicrob Agents Chemother. 2011; doi: 10.1128/AAC.01764-10
26. Förster A, Hill CP. Proteasome Activators. Protein Degrad. 2007; 2 :89–110.

Europe PMC Funders Author Manuscripts

27. Huber EM, Groll M. The Mammalian Proteasome Activator PA28 Forms an Asymmetric α4β3 Complex. Structure. 2017; 25 :1473–1480. e3 [PubMed: 28867616]
28. Kuehn L, Dahlmann B. Proteasome activator PA28 and its interaction with 20 S proteasomes. Arch Biochem Biophys. 1996; 329 :87–96. [PubMed: 8619639]
29. Benaroudj N, Zwickl P, Seemüller E, Baumeister W, Goldberg AL. ATP hydrolysis by the proteasome regulatory complex PAN serves multiple functions in protein degradation. Mol Cell. 2003; doi: 10.1016/S1097-2765(02)00775-X
30. Huang R, et al. Unfolding the mechanism of the AAA+ unfoldase VAT by a combined cryo-EM, solution NMR study. Proc Natl Acad Sci U S A. 2016; 113 :E4090–W4199.
31. Ripstein ZA, Huang R, Augustyniak R, Kay LE, Rubinstein JL. Structure of a AAA+ unfoldase in the process of unfolding substrate. Elife. 2017; 6 :1–14.
32. Gerega A, et al. VAT, the Thermoplasma homolog of mammalian p97/VCP, is an N domain-regulated protein unfoldase. J Biol Chem. 2005; doi: 10.1074/jbc.M510592200
33. Akopian TN, Kisselev AF, Goldberg AL. Processive degradation of proteins and other catalytic properties of the proteasome from Thermoplasma acidophilum. J Biol Chem. 1997; 272 :1791–1798. [PubMed: 8999862]
34. Pédelacq JD, Cabantous S, Tran T, Terwilliger TC, Waldo GS. Engineering and characterization of a superfolder green fluorescent protein. Nat Biotechnol. 2006; 24 :79–88. [PubMed: 16369541]
35. Ward WW, Prentice HJ, Roth AF, Cody CW, Reeves SC. Spectral Perturbations of the Aequorea Green-Fluorescent Protein. Photochem Photobiol. 1982; 35 :803–808.
36. Hsu S-TD, Blaser G, Jackson SE. The folding{,} stability and conformational dynamics of β-barrel fluorescent proteins. Chem Soc Rev. 2009; 38 :2951–2965. [PubMed: 19771338]
37. Kisselev AF, Songyang Z, Goldberg AL. Why does threonine, and not serine, function as the active site nucleophile in proteasomes? J Biol Chem. 2000; 275 :14831–14837. [PubMed: 10809725]
38. Biesemans A, Soskine M, Maglia G. A Protein Rotaxane Controls the Translocation of Proteins Across a ClyA Nanopore. Nano Lett. 2015; 15 :6076–6081. [PubMed: 26243210]
39. Majumder P, et al. Cryo-EM structures of the archaeal PAN-proteasome reveal an around-the-ring ATPase cycle. Proc Natl Acad Sci U S A. 2019; doi: 10.1073/pnas.1817752116
40. Kisselev AF, Akopian TN, Goldberg AL. Range of sizes of peptide products generated during degradation of different proteins by archaeal proteasomes. J Biol Chem. 1998; doi: 10.1074/jbc.273.4.1982
41. Maglia G, Heron AJJ, Stoddart D, Japrung D, Bayley H. Analysis of single nucleic acid molecules with protein nanopores. Methods Enzym. 2010; 475 :591–623.

Europe PMC Funders Author Manuscripts

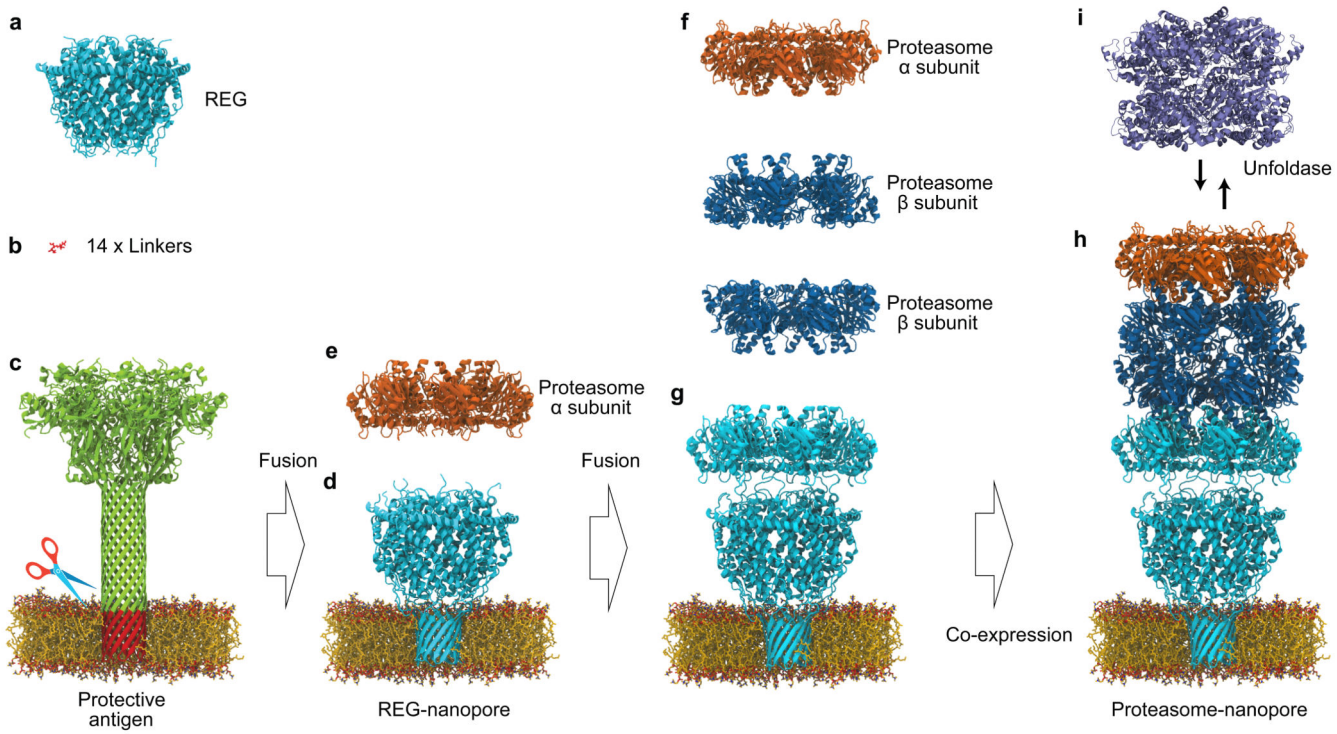

Fig. 1. Design of a proteasome nanopore.

a, Structure of mouse REG (PDB ID: 5MSJ). **b**, Sticks diagram of the structure of serine-serine-glycine linker. **c**, Ribbon diagram of the structure of anthrax protective antigen (PDB ID: 3J9C). The transmembrane region of the protective antigen is in red. **d**, Structure of the REG-nanopore enhanced by molecular dynamics simulations. REG (**a**) was genetically fused to the transmembrane region of the protective antigen (**c**) *via* a short linker (**b**). **e** and **f**, Structure of the *T. acidophilum* proteasome α-and β-subunit (PDB ID: 1YA7). **g**, REG-nanopore was genetically fused to α-subunit of *T. acidophilum* proteasome. **h**, Structure of the designed proteasome-nanopore refined by MD simulations. **i**, Structure of VATΔN (PDB ID: 5G4G).

Europe PMC Funders Author Manuscripts
Europe PMC Funders Author Manuscripts

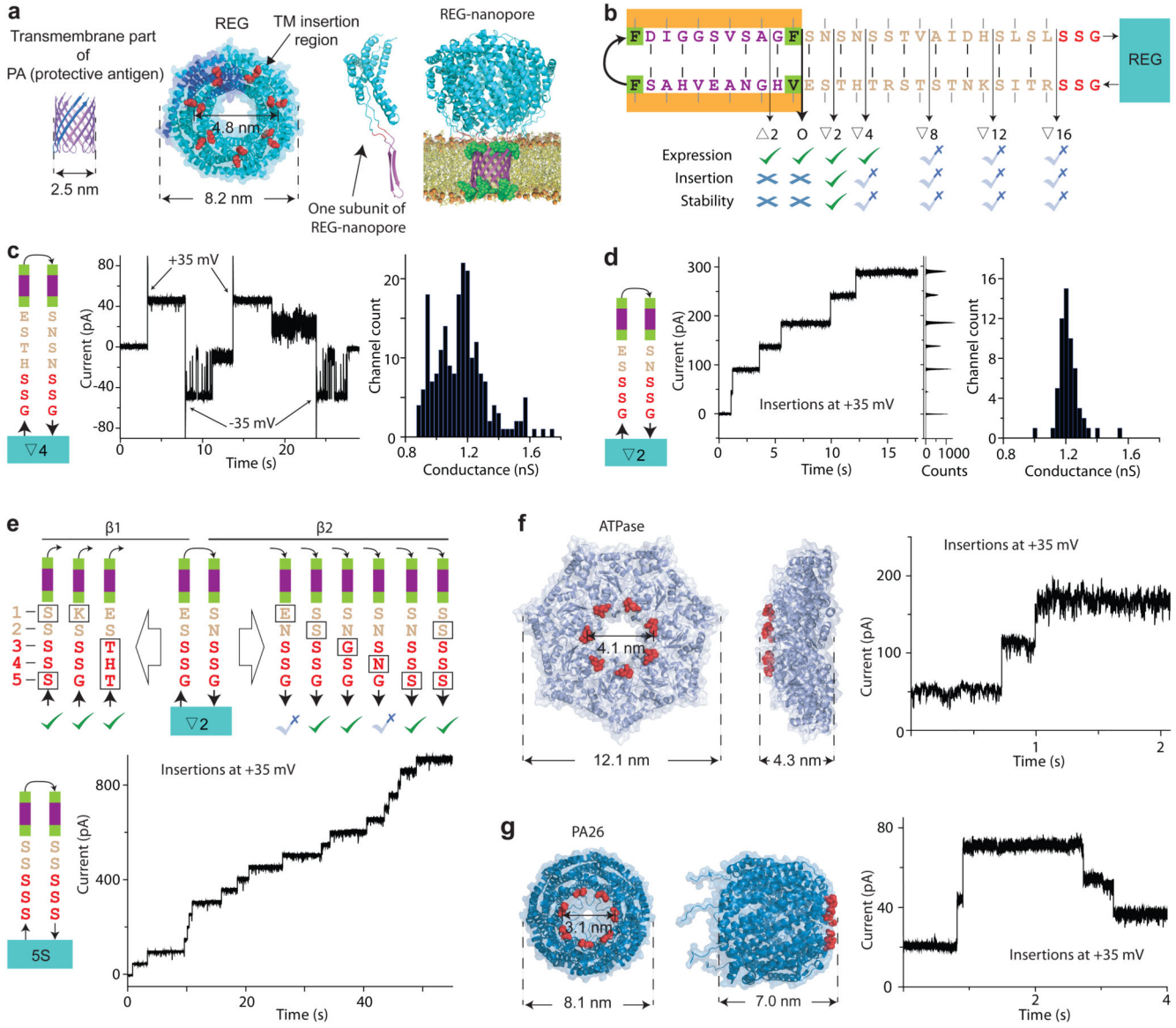

Fig. 2. Fabrication and optimization of the artificial nanopores.

a, Structural representation of the designed nanopores. The heptameric transmembrane part of protective antigen (PA) replaced an unstructured loop (red) in REG (cyan). One subunit in the transmembrane region and REG is highlighted in blue and showed in isolation. The hydrophobic residues anchoring the nanopore to the membrane are indicated in green. The REG-nanopore was generated by molecular dynamics simulations. **b**, Effects of linker length on the nanopore expression in *E. coli.* cells, insertion efficiency and nanopore stability. The side chains that point towards the outside and inside of the barrel are highlighted with grey and black lines, respectively. The first designed nanopore (0) is highlighted with a wider arrow. One deletion mutant (Δ2) and five insertion mutants (∇2, ∇4, ∇8, ∇12, and ∇16) were tested. The sequence of the protective antigen was used as template for the linker. REG is shown as a cyan rectangle. **c, d** Electrical properties of the functional ∇4 (**c**) and ∇2 (**d**) mutants. On the left is sequence of the mutant, in the middle a typical current trace, and

Europe PMC Funders Author Manuscripts
Europe PMC Funders Author Manuscripts

on the right the current histogram corresponding the insertions of multiple pores at +35 mV. **e**, top, linker optimization tested by substituting several residues. Bottom, Electrical properties of a REG-nanopore with homo-polymeric serine linkers. **f**, ATPase-nanopore formed by introducing the transmembrane barrel elongated with the homo-polymeric serine linkers within a loop (red) at the AAA+ ATPase domain of *Trypanosoma brucei* σ54-RNA polymerase. **g**, Formation of a PA26-nanopore by introducing the β-barrel elongated by the serine linker into a loop in the top face of PA26 from *Aquifex aeolicus.* Electrical data were collected at ±35 mV in 1 M NaCl, 15 mM Tris, pH 7.5, using 10 kHz sampling rate and a 2 kHz low-pass Bessel filter.

Europe PMC Funders Author Manuscripts

Europe PMC Funders Author Manuscripts

Europe PMC Funders Author Manuscripts

Europe PMC Funders Author Manuscripts

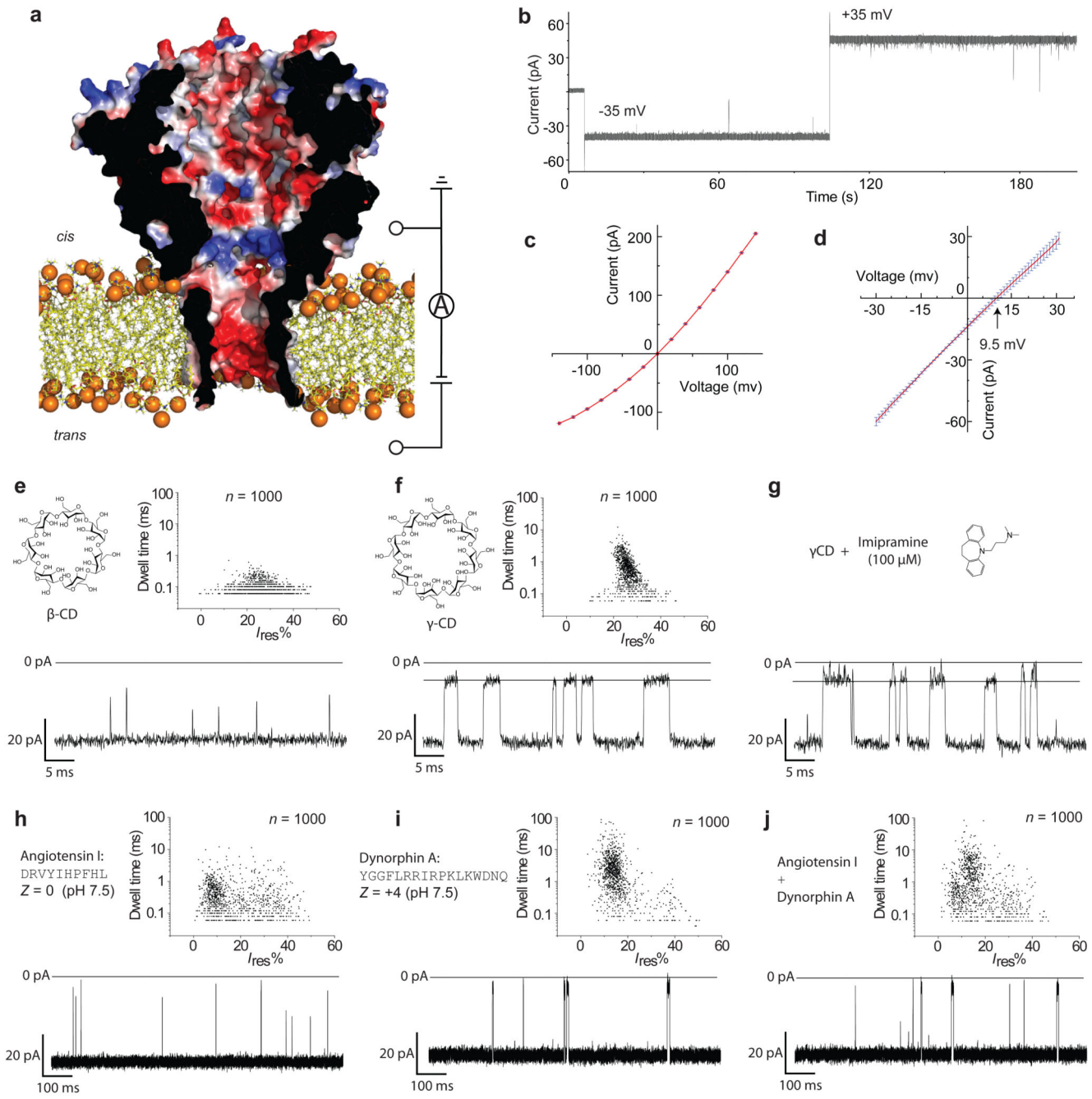

Fig. 3. Electrical properties of REG-nanopore.

a, Cut-through of a surface representation of REG-nanopore. The pore is coloured according to the vacuum electrostatic potential as calculated by PyMOL on the final snapshot of the multiscale MD model. **b**, A typical current trace recorded of a single REG-nanopore at +35 and -35 mV. **c**, Current–voltage (*I*−*V*) characteristics of three different nanopores. **d**, Reversal potential measured using asymmetric ion concentrations (*trans*:*cis*, 0.5 M NaCl: 2.0 M NaCl), showing that the pore is cation-selective, as expected from the electrostatic potentials of the nanopore lumen. The REG-nanopore was added to the *trans* side. **e-f**,

Europe PMC Funders Author Manuscripts

Europe PMC Funders Author Manuscripts

Chemical structure of β-CD (**e**) and γ-CD (**f**) (left), scatter plots of I_{res}% versus dwell time (right), and representative trace of 20 μM β-CD (**e**) and 20 μM γ-CD (**f**) blockades (below). **g**, Chemical structure of imipramine and a representative trace of γ-CD cyclodextrin blockades (20 μM) in the presence of 100 μM of imipramine. **h-j**, typical peptide blockades (bottom) and resulting scatter plots of I_{res}% versus dwell time (top) for 4 μM of angiotensin I (**h**) 4 μM dynorphin A (**i**) and a 2 μM equimolar mixture of the two (**j**). The REG-nanopore and all analytes were added to the *cis* side. Electrical recordings were collected at -35 mV in 1 M NaCl, 15 mM Tris, pH 7.5. All traces except (**b**) were sampled at 50 kHz sampling rate and a 10 kHz low-pass Bessel filter, and an additional Gaussian low-pass filter with a 5 kHz cut-off was digitally applied. In **b**, data were collected at 10 kHz sampling rate and a 2 kHz low-pass Bessel filter.

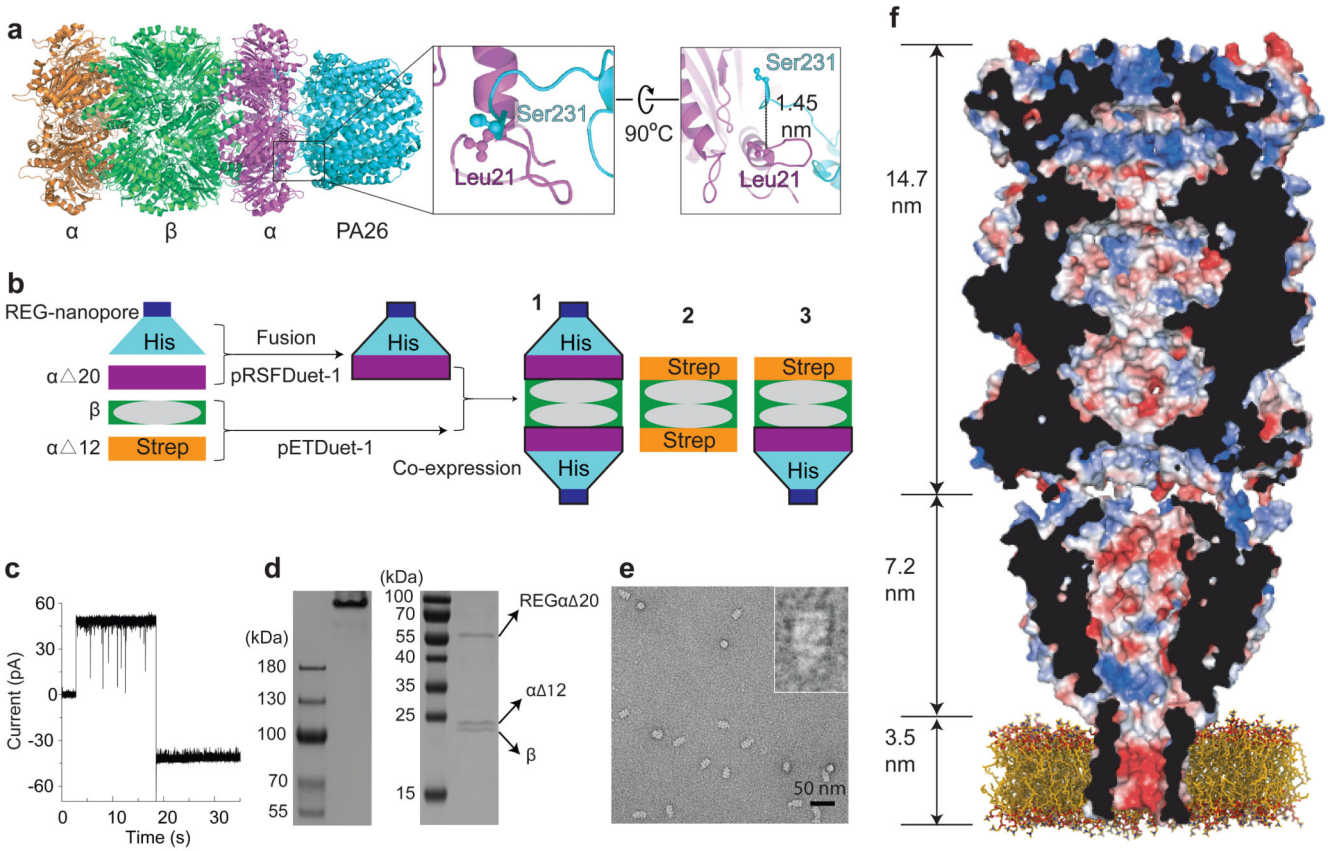

Fig. 4. Design of the artificial proteasome-nanopore.

a, Structure of the *T. acidophilum* proteasome (the α-subunit is orange and magenta, the β-subunit is green) in complex with PA26 (cyan). The C-terminal of PA26 (S231) is near L21 of the proteasome α-subunit. **b**, A representation of the reconstitution of the artificial proteasomal nanopore. To obtain complex **3**, two separate vectors were used to express the three proteins. The REG-nanopore was fused to the proteasome α-subunit and contained a His-tag. The protein was co-expressed with the untagged β-subunits and a second α-subunit containing a Strep-tag. His-tag affinity chromatography was used to co-purify complex **1** and **3**. Then a Strep-Tag affinity chromatography was used to purify **3**. **c**, Electrical behaviour of a single pore at ±35 mV in 1 M NaCl, 15 mM Tris, pH 7.5, using 10 kHz sampling rate and a 2 kHz low-pass Bessel filter. **d**, Native PAGE (left, ~5 μg) and SDS-PAGE (right, ~2 μg) analyses of the purified complex **3**. SDS-PAGE revealed the presence of three unique bands corresponding well the molecular weights of REGαΔ20, proteasome αΔ12-subunit, and proteasome β-subunit (51.8, 25.9, and 22.3 kDa). The native PAGE showed that REGαΔ20, proteasome αΔ12-subunit, and proteasome β-subunit form a stable complex **3**. **e**, TEM image of the proteasome-nanopore. **f**, Cut-through of a surface representation of proteasome-nanopore enhanced by molecular dynamics simulations and coloured (blue, positive; red, negative) according to the vacuum electrostatic potential as calculated by PyMOL.

Europe PMC Funders Author Manuscripts
Europe PMC Funders Author Manuscripts

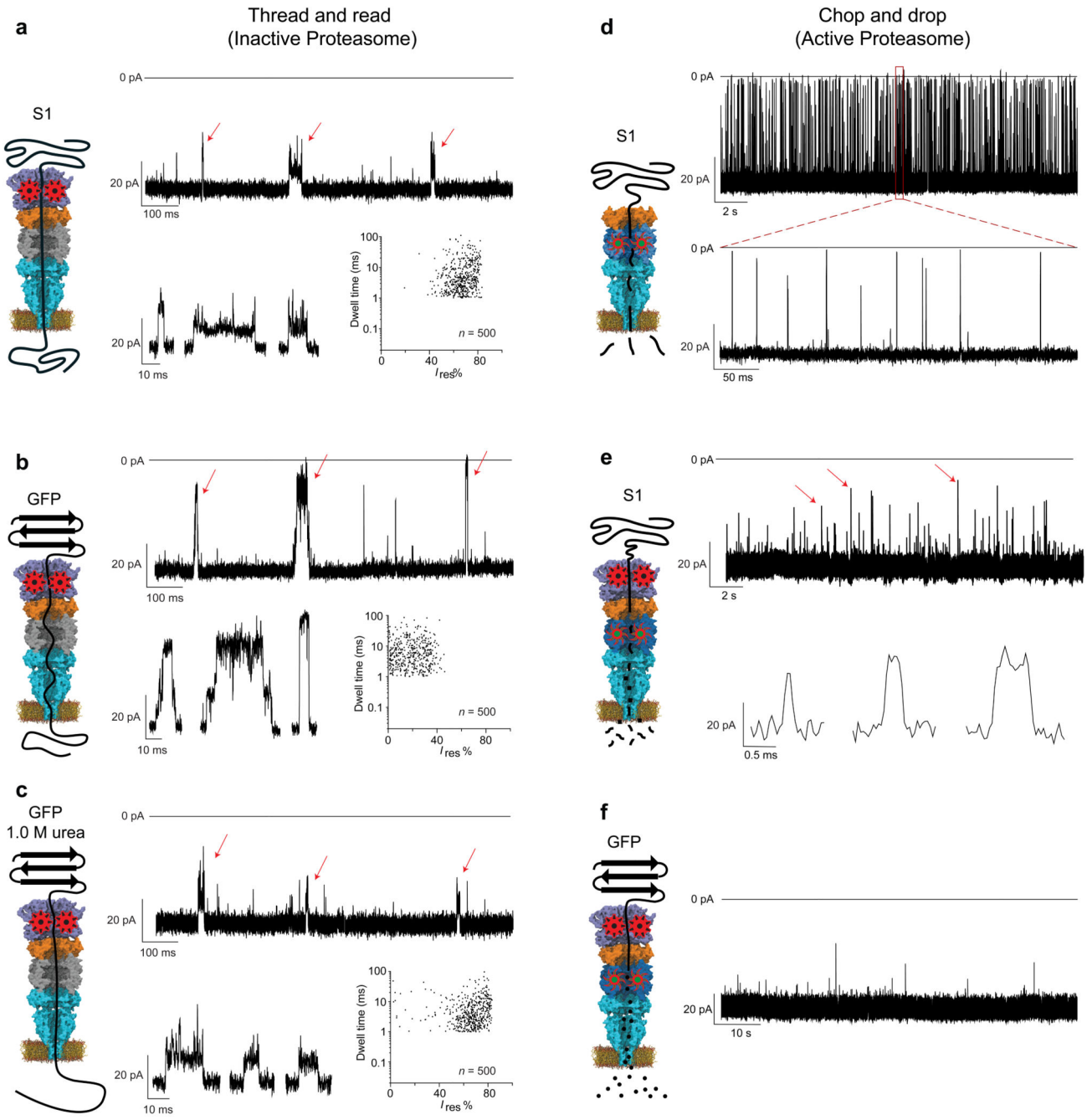

Fig. 5. Controlled translocation through the proteasome-nanopore. a-c, Thread-and-read. Typical current traces and relative scatter plots showing the average I_{res}% versus dwell time provoked by the translocation of S1 (**a**, 20.0 μM S1 and 20.0 μM VAT, 23 independent nanopore experiments), GFP (**b**, 5.0 μM and 5.0 μM VATΔN, 42 independent experiments), and GFP in 1 M urea (**c**, 5.0 μM and 5.0 μM VATΔN, 13 independent experiments) through an inactive proteasome-nanopore mediated by VATΔN in the presence of 2.0 mM ATP. The proteasome-nanopore and substrates were added to the *cis* side. **d-f, Chop-and-drop**. Typical current traces provoked by the transport of oligopeptides across an activated

Europe PMC Funders Author Manuscripts
Europe PMC Funders Author Manuscripts

proteasome. **d**, Unassisted S1 translocation (>50 independent experiments). **e**, VATΔN and ATP assisted S1 transport induce fragmentation into small peptides, which fast transport is seldomly observed (23 independent experiments). **f**, VATΔN assisted GFP-ssrA proteolytic cleavages produce peptides that are too short to be detected by the nanopore (15 independent experiments). Data were collected at 40°C and -30 mV in 1 M NaCl, 15 mM Tris, pH 7.5, using a 10 kHz low-pass Bessel filter with a 50 kHz sampling rate. The traces were then filtered digitally with a Gaussian low-pass filter with a 5 kHz cutoff.

Europe PMC Funders Author Manuscripts

Europe PMC Funders Author Manuscripts